NANO LETTERS

Letter

Single Sub-20 nm Wide, Centimeter-Long Nanofluidic Channel Fabricated by Novel Nanoimprint Mold Fabrication and Direct Imprinting

Xiaogan Liang, Keith J. Morton, Robert H. Austin, and Stephen Y. Chou

Nano Lett., **2007**, 7 (12), 3774-3780• DOI: 10.1021/nl072253x • Publication Date (Web): 01 November 2007

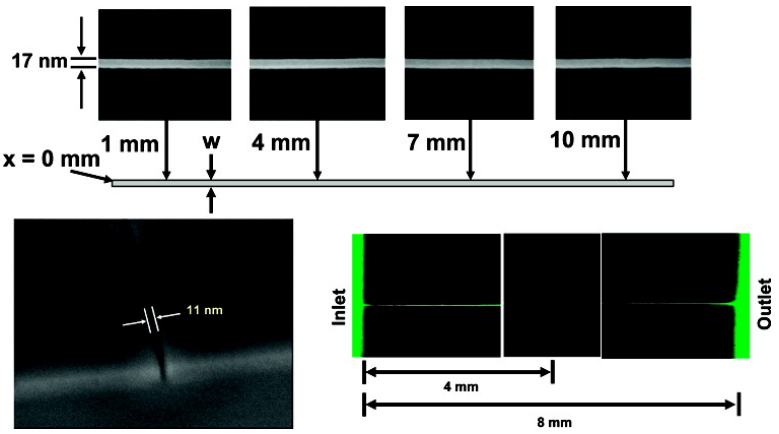

More About This Article

Additional resources and features associated with this article are available within the HTML version:

- Supporting Information
- Links to the 7 articles that cite this article, as of the time of this article download
- Access to high resolution figures
- Links to articles and content related to this article
- Copyright permission to reproduce figures and/or text from this article

View the Full Text HTML

NANO LETTERS

2007
Vol. 7, No. 12
3774−3780

Single Sub-20 nm Wide, Centimeter-Long Nanofluidic Channel Fabricated by Novel Nanoimprint Mold Fabrication and Direct Imprinting

Xiaogan Liang,[†] Keith J. Morton,[†] Robert H. Austin,[‡] and Stephen Y. Chou*[,†]

Nanostructure Laboratory, Department of Electrical Engineering, Department of Physics, Princeton University, Princeton, New Jersey 08544

Received September 4, 2007; Revised Manuscript Received October 19, 2007

ABSTRACT

We report and demonstrate a new method to fabricate single fluidic-channels of uniform channel width (11−50 nm) and over 1.5 cm in length, which are essential to developing innovative bio/chemical sensors but have not been fabricated previously. The method uses unconventional nanofabrication (a combination of crystallographic anisotropic etching, conformal coating, and edge patterning, etc.) to create an imprint mold of a channel pattern and nanoimprint to duplicate such channel. The centimeter-long channel continuity is verified by flowing fluorescent dye-stained water and stretching and transporting DNAs. The 18 by 20 nm channel cross-section was confirmed by measuring the liquid conductance in the channel.

One critical challenge in developing many innovative bio/chemical sensors is the fabrication of a single narrow yet long (centimeter) and continuous fluidic channel at the precisely designated location.[1−7] Such channels of a sub-20 nm width, essential for device function, were hardly fabricated previously because of the intrinsic limitations in the fabrication methods used, particularly the traditional nanofabrication methods (e.g., writing and etching nanostructures).[8−10] For example, to explore a new real-time DNA-sequencing device (potentially revolutionary if successful), it requires not only a continuous fluidic channel of a width below 20 nm and a length of a centimeter for stretching and stabilizing DNAs, but also a single channel host for putting electrical or optical sensors inside the channel.[4,5,7,11−15] Multiple channels will greatly complicate the sensor fabrication and the addressable detection of single DNA.[15,16] These requirements make the fabrication of a single sub-20 nm wide, centimeter-long, continuous fluidic channel extremely challenging due to two main reasons. (a) All scanning nanostructure-writing tools, such as electron beam lithography, ion beam lithography, or scanning probe patterning are limited to a writing field of ∼100 μm for sub-20 nm structures, which is not sufficient for the needed long channel. Stitching of different fields does not have the necessary accuracy to connect two channels into a single continuous channel. All the nanostructure-writing tools based on a fixed writing beam (probe) and a moving stage can barely maintain sub-20 nm writing over centimeter distances. (b) Because of the noise in these writing tools and reactive ion etching (if used), the line-edge-roughness (LER), which has an average size of 5−50 nm, will clog the channel before the average channel width is reduced to 20 nm, because just one large edge variation (far larger than average) can clog the long channel. Interference lithography can make narrow continuous fluidic-channels over centimeter lengths but it usually makes dense, multiple channels rather than a single channel,[15] and it also suffers LER as nanostructure writing tools, preventing a small needed channel width (in principle, a single channel line may be produced by interference lithography under special conditions).

Previously, a number of works have been carried out to achieve the narrow single channel or multiple channels. For examples, multiple channels of a width down to 35 nm have been fabricated by interference lithography without additional size shrinking.[17] Single channels have been fabricated by using edge patterning[18] (note: edge patterning has shown features of 7 nm),[19] sacrificial electrical-spinning fiber,[20−22] and further reduction of the microchannels by the shadow evaporation[3,23−25] and oxidation.[26] Some of the methods can make a single centimeter-long channel, but sidewall edge roughness clogs a channel before the channel width gets small. An electrospinning fiber might not suffer the edge roughness, but it is very difficult to position the fiber

* Corresponding author. E-mail: chou@princeton.edu.
[†] Nanostructure Laboratory, Department of Electrical Engineering.
[‡] Department of Physics.

10.1021/nl072253x CCC: $37.00
Published on Web 11/01/2007

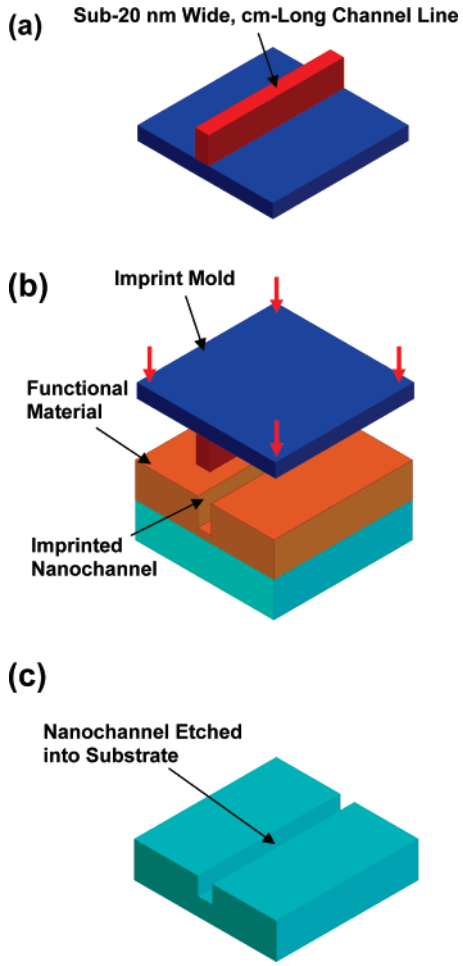

Figure 1. Schematic of key steps in the fabrication of a single narrow, centimeter-long continuous fluidic channel with uniform channel width. (a) Formation of an imprint mold having a single sub-20 nm wide, centimeter-long, continuous channel; (b) direct imprinting of functional materials; and (c) optional pattern transfer into the underlying substrate by RIE.

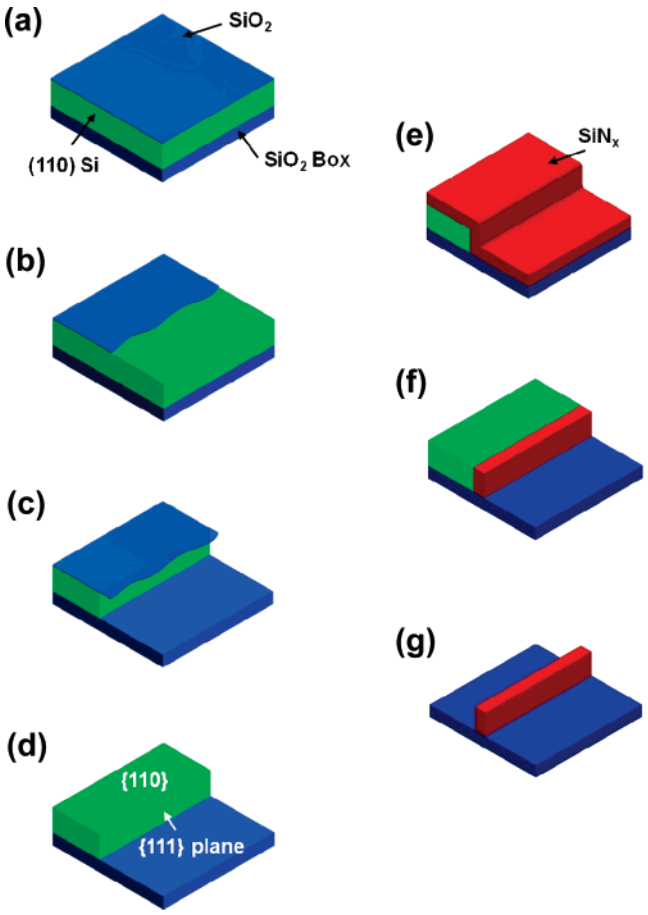

Figure 2. Schematic of the fabrication steps for making an imprint mold bearing a single, narrow long, uniform width fluidic channel without using nanostructure writing tools nor nanostructure RIE. (a) Thermal oxidation to form SiO_2 on (110) Si surface of a SOI wafer. (b) Photolithography and RIE patterning of a large rectangle (1.5 cm × 0.5 cm) in SiO_2 with the longer edge aligned to {111} crystallographic axis. (c) Crystallographic anisotropic etching of (110) Si using the SiO_2 mask. (d) Removal of SiO_2 mask. (e) Conformal LPCVD of Si_xN_y. (f) CHF_3/O_2 RIE to etch away the Si_xN_y on top of the Si mesa and wafer (but not the sidewall) (g) Removal of (110) Si to create a free-standing Si_xN_y protrusive wall. Other patterning process cuts the Si_xN_y wall into a single, narrow, long, uniform width channel pattern line on the mold.

precisely for building the rest of the parts of the nanometer-scale sensors. Because of these limitations, a precisely positioned single sub-20 nm wide, centimeter-long continuous fluidic channel has not been achieved.

To overcome all these limitations, here we report and demonstrate a new approach[27] for making a single, sub-20 nm wide yet centimeter-long and continuous fluidic channel. The new approach has three key steps (Figure 1): (a) an innovative mold fabrication that creates a nanoimprint mold having a single sub-20 nm wide, centimeter-long, continuous fluidic channel integrated with other nano/microstructures necessary for a bio/chemical analysis; (b) use of the mold to faithfully imprint the nanochannel line in a functional material layer; and (c) an optional RIE that transfers the imprinted patterns into a substrate.[27−30] The novel mold fabrication does not use any nanostructure writing nor need RIE to etch nanostructures; rather it uses anisotropic etching of crystalline planes,[28] conformal deposition, and edge definition to create a narrow long continuous channel on an imprint mold and uses NIL to duplicate the patterns on a mold with nanometer fidelity.[29,30] Because the crystalline anisotropic etching removes the sidewall edge roughness (to achieve atomic smoothness) and the conformal edge definition guarantees the channel width uniformity, such an approach can guarantee the channel width uniformity and sidewall smoothness over the entire channel length, hence ensuring a successful fabrication of a single narrow, long, continuous fluidic channel.

The detailed steps of the mold fabrication are shown schematically in Figure 2: (a) A thin layer of SiO_2 (~10 nm) is grown on a (110)-oriented silicon-on-insulator (SOI) wafer by thermal oxidation. (b) Photolithography patterns a 0.5 cm × 1.5 cm rectangle pattern in the SiO_2 layer with the longer edges of rectangles aligned to {111} crystallographic axis of the (110) Si, followed with RIE of the SiO_2. (c) After stripping photoresist, the SiO_2 rectangle pattern is used as an etching mask to etch the (110) Si layer by an anisotropic wet etching (e.g., KOH). Because the etching rate of crystalline silicon in the <111> direction is much slower than that in the <110> directions, the anisotropic

chemical etching creates a Si mesa with two vertical sidewalls of {111} planes with nearly atomic-scale smoothness even if the original SiO_2 etch mask has severe edge roughness. (d) The top SiO_2 mask layer is stripped away. (e) Si_xN_y is deposited by low-pressure chemical vapor deposition (LPCVD) to conformably and uniformly cover the entire wafer surface including the Si mesa sidewalls. (f) A RIE etches Si_xN_y anisotropically in the vertical direction, removing all Si_xN_y on the mesa and wafer, but keeping some Si_xN_y on the sidewall (because the sidewall height is larger than the Si_xN_y thickness). (g) The Si mesa is selectively etched away, leaving a narrow, long, continuous Si_xN_y sidewall on SiO_2 surface, forming the protrusion of an imprint mold. (h) Optionally using other patterning steps, the auxiliary parts of the device (e.g., inlet and outlet of fluidic channel) are added on the mold (not shown in Figure 2). Finally, the mold surface is chemically treated with the mold release agent and is ready for nanoimprint lithography.

In comparison with previous edge patterning and dimensional transfer methods,[18,19] the novel mold fabrication offers several unique advantages: (i) the anisotropic etching of (110) Si ensures a nearly atomically smooth sidewall over several centimeters length, regardless of initial edge roughness caused by lithography.[28] (ii) The channel width on the mold is defined by the LPCVD film thickness, which can be sub-10 nm thick with nearly atomic resolution, rather than by lithography. And (iii) The conformal deposition ensures a uniform channel width (hence continuity) over entire channel length, regardless the sidewall roughness.

In one of our mold fabrications, the mold substrate, (110)-oriented SOI substrate (Silicon Quest International, Inc.), had a 2 μm thick Si layer on a 1 μm thick buried oxide layer. The Si layer was carefully thinned from 2 μm to tens of nanometers by alternate thermal oxidation and hydrofluoric acid etching. The thickness of the (110)-oriented silicon layer was monitored and mapped by a Nanospec tabletop film analysis system (Nanometrics, Inc.). The final thickness variation of the Si layer is measured to be less than 5 nm over a centimeter-long length. The anisotropic (110) Si etchant is a mixture of 125 g of potassium hydroxide (KOH), 400 mL of deionized (DI) water, and 100 mL of electronic grade isopropyl alcohol (IPA), and the etching was performed at 65 °C. A scanning electron microscopic (SEM) image clearly shows that the SiO_2 edges, patterned by photolithography and etching, are rough with a LER (3σ) in 100's nm (Figure 3a), but the edges of anisotropically etched (110) Si is nearly atomically smooth and vertical (Figure 3b after stripping the oxide mask in diluted HF ($\sim$2%)). Although there was an etching back of silicon underneath the oxide mask ($\sim$100 nm), it does not affect the position precision of the single nanochannel relative to other nanostructures, because we fabricate the channel first (using the mold) and then precisely align other structures with the channel using alignment marks and the corrections to the etch-back.

To create the final narrow and long channel pattern on the mold, LPCVD conformably coats a Si_xN_y layer over the Si mesa, followed by a CHF_3/O_2 RIE. LPCVD was performed in a Tystar Tytan tube furnace ($T = 780$ °C, $P = 10$ mTorr, gas flow: 50 sccm dichlorosilane; 150 sccm ammonia), and the resultant Si/N ratio is about 3:4. Excellent conformity and durability of Si_3N_4 as a mold material were verified by following SEM imaging and imprint tests, respectively. Finally, all Si mesas were removed by a KOH-based etchant, leaving a sub-20 nm wide Si_xN_y protrusive line over 1.5 cm long length on the surface of the mold. Figure 3c shows a cross-sectional SEM image of a mold bearing a $\sim$17 nm wide 1.5 cm long protrusive nanochannel pattern. The smooth and vertical sidewalls of the mold are attributed to the nature of crystallographic anisotropic etching of (110) Si surface and conformal LPCVD of Si_xN_y. More importantly, as pointed out earlier, this novel mold fabrication ensures a continuous and uniform channel over a centimeter scale length even if the channel sidewalls have roughness. Figure 3d shows that the sidewall has a nanometer scale kink shift created in the Si etching due to a slight misalignment between the {111} crystallographic axis and the SiO_2 mask edge, but the channel line width is still uniform and continuous.

In imprinting, the mold was pressed into a UV-curable material layer (Nanonex NXR-3020) using a nanoimprinter (Nanonex NX-2000), which has an Air Cushion Press that allows uniform imprint over an entire wafer. The imprinted nanochannel itself can be directly used as a fluidic-channel for bio/chemical analysis. Alternatively, the imprinted structures can be used as an etching mask to faithfully transfer the channel into the underlying substrate such as SiO_2 in a RIE process. Because RIE is used only once in this optional approach, the edge roughness can be minimized. Here, we used a brief O_2-based RIE to etch away the NXR-3020 residual layer for exposing the underlying SiO_2 surface and then a CF_4-based RIE to transfer the channel into the SiO_2. Figure 3e shows the cross-sectional SEM image of a single 11 nm wide, 1.5 cm long nanochannel in SiO_2 fabricated using this method.

Using SEM, we studied the channel width uniformity over the entire channel length of the imprint mold, the imprinted channel, and the etched channel. The imprint mold was coated with 1 nm thick iridium for avoiding the charging effect during SEM imaging. Figure 4a shows the top-view of four SEM images of a 1.5 cm long protrusive nanochannel line on an imprint mold captured at 1, 4, 7, and 10 mm locations of the channel, respectively, demonstrating an excellent channel width uniformity. Using digitized SEM image and Fractal analysis,[31] we found the average line width is 17 nm, and the 3σ-LER is 1.6 nm over a 1.5 cm channel length (note: SEM image has a resolution better than 1 nm/pixel). Figure 4b shows the SEM images of the imprinted nanochannel in a NXR-3020 layer using the mold shown in Figure 4a. Data analysis shows that the imprinted channel has the same average channel as the mold (17 nm), but the 3σ-LER increased to 3 nm. Figure 4c shows the SEM images of the nanochannel etched into SiO_2 using the imprinted channel layer as an etching mask. The etching depth is 20 nm. Data analysis shows that the average channel width of the etched nanochannel is 18 nm, which is 1 nm wider than its etching mask, and the 3σ-LER increased to 6 nm over a

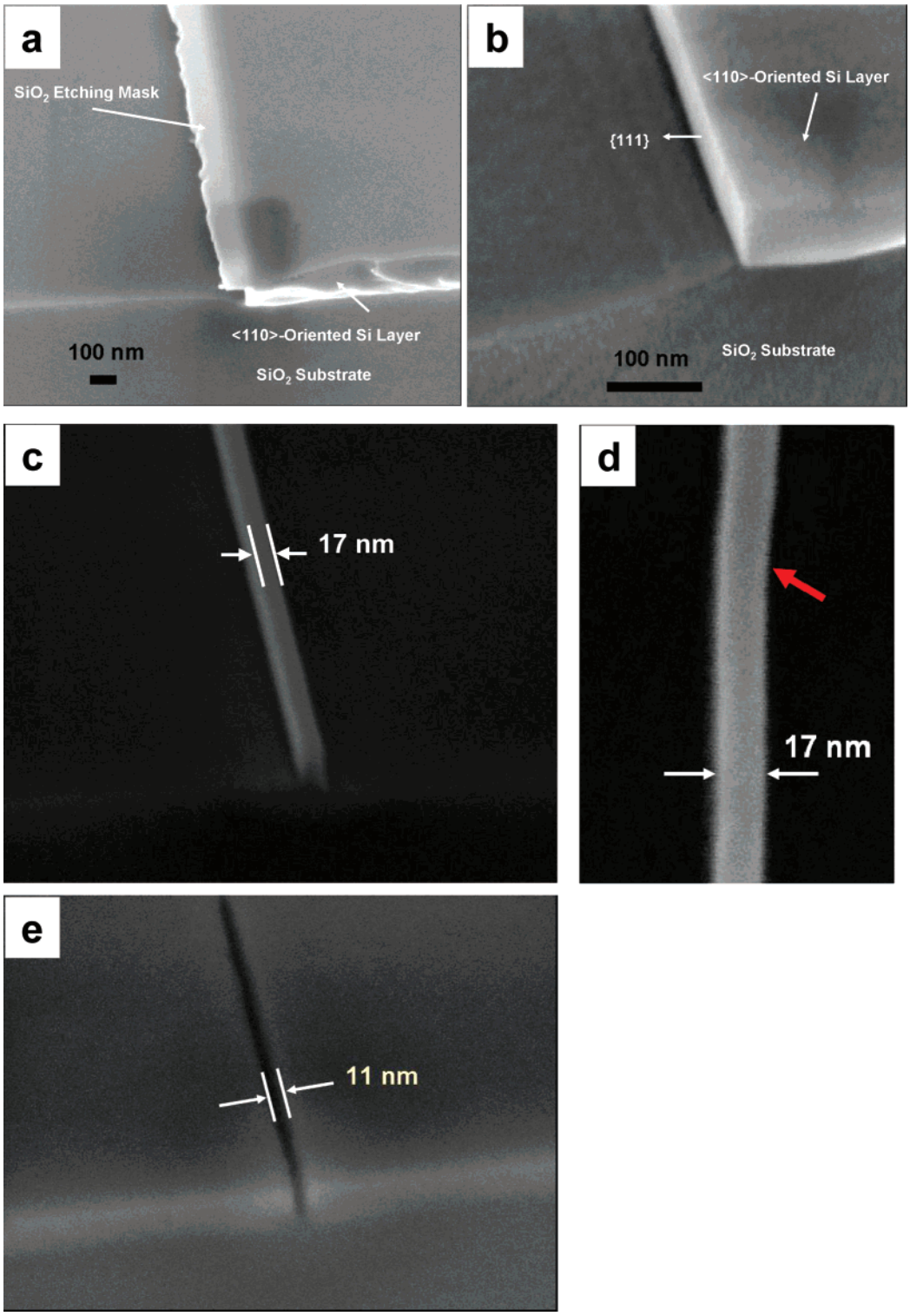

Figure 3. (a) Anisotropically etched edge in (110)-oriented SOI before the removal of SiO_2 mask. Note the rough edge in the SiO_2 mask layer. (b) The smooth, vertical, and straight edge in (110) SOI after the removal of SiO_2 mask. (c) The cross-sectional SEM image of an imprint mold bearing a 17 nm wide 1.5 cm long single nanochannel pattern line. (d) The SEM image of a segment of the channel line, which indicates that even with a tiny kink shift induced by the misalignment with {111} crystallographic axis, the channel line is still continuous and uniform. (e) The cross-sectional SEM image of an 11 nm wide, 1.5 cm long nanochannel etched in SiO_2.

1.5 cm length. These data clearly demonstrate that the new approach indeed offers sub-10 nm lithographic resolution for patterning sub-20 nm channel line with a great width uniformity over a centimeter-scale channel length.

To complete a nanofluidic device, after the channel fabrication a pair of liquid reservoirs for connecting the nanochannel was made by photolithography and RIE. Then the accessing holes (~1 mm diameter) to the liquid reservoirs were drilled by a sandblasting tool (Danville Engineering, Inc.). The whole chip was sealed by a 1 in.^{2} Pyrex glass cover slip (0.17 mm thick). Before sealing, both the channel substrate and the cover slip were cleaned by standard RCA-I

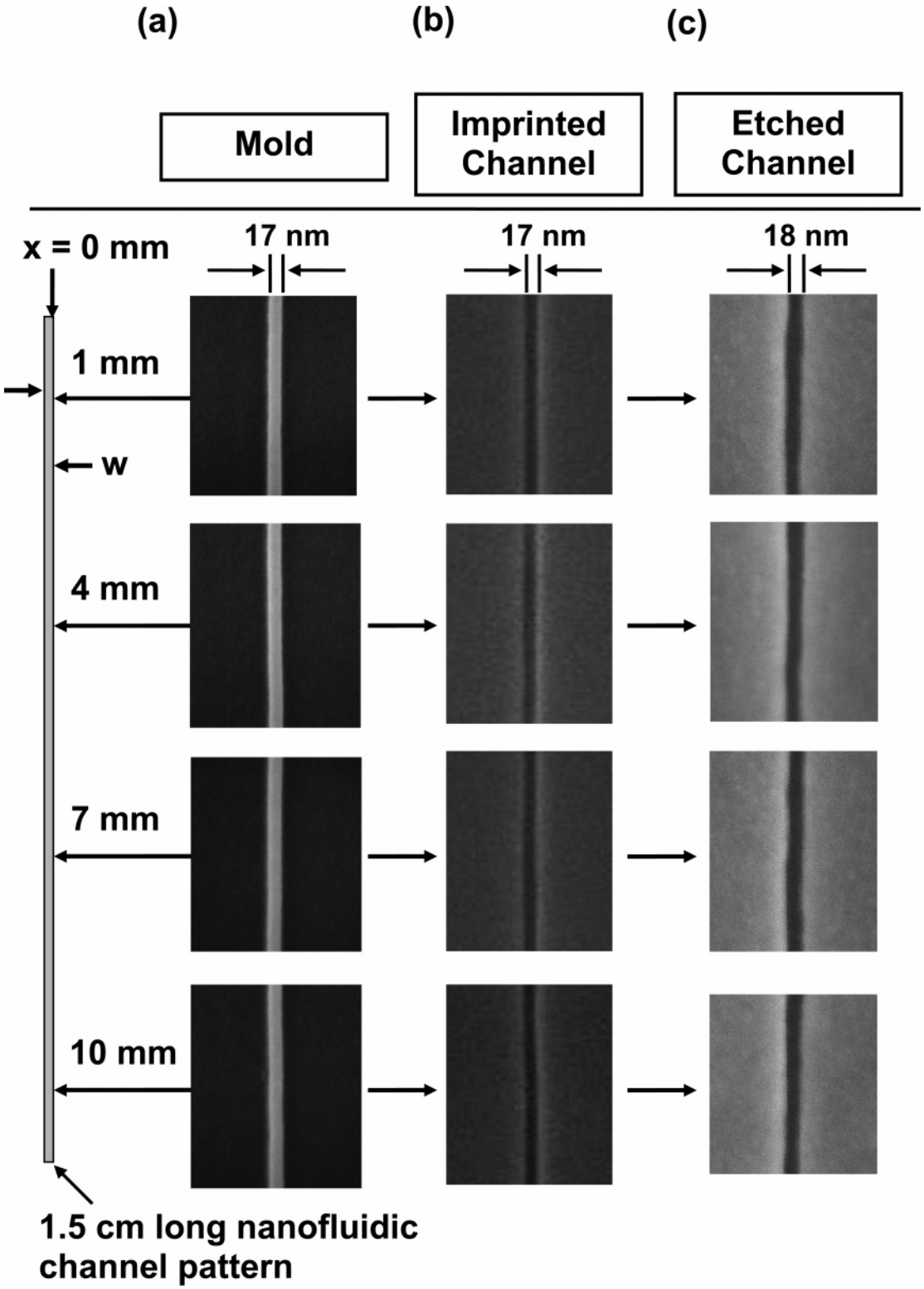

Figure 4. Top-down SEM images of (a) a 17 nm wide, 1.5 cm long single nanochannel pattern on an imprint mold (3σ error = 1.6 nm); (b) the corresponding 17 nm wide, 1.5 cm long nanochannel directly imprinted in a NXR-3020 UV-curable functional material layer (3σ error = 3 nm); (c) the 18 nm wide, 1.5 cm long nanochannel subsequently etched in SiO_2 by RIE (3σ error = 6 nm).

and RCA-II procedures and subsequently activated by O_2 plasma. Finally, the sealing is finished by bringing the substrate and the cover slip into a firm contact.

To demonstrate that the narrow centimeter-long nanochannel is indeed continuous over the entire length, we performed two tests: flowing colored wafer and flowing DNA in solution. In the colored water test, the DI water containing fluorescent dye (10 mg/mL solution of closely neutral rhodamine B in a 50% mixture of methanol and deionized water, pH ~7.0) was filled into a 30 nm wide, 8 mm long enclosed channel by capillary action. Figure 5a shows the fluorescent images captured at the inlet (x = 0 mm), the

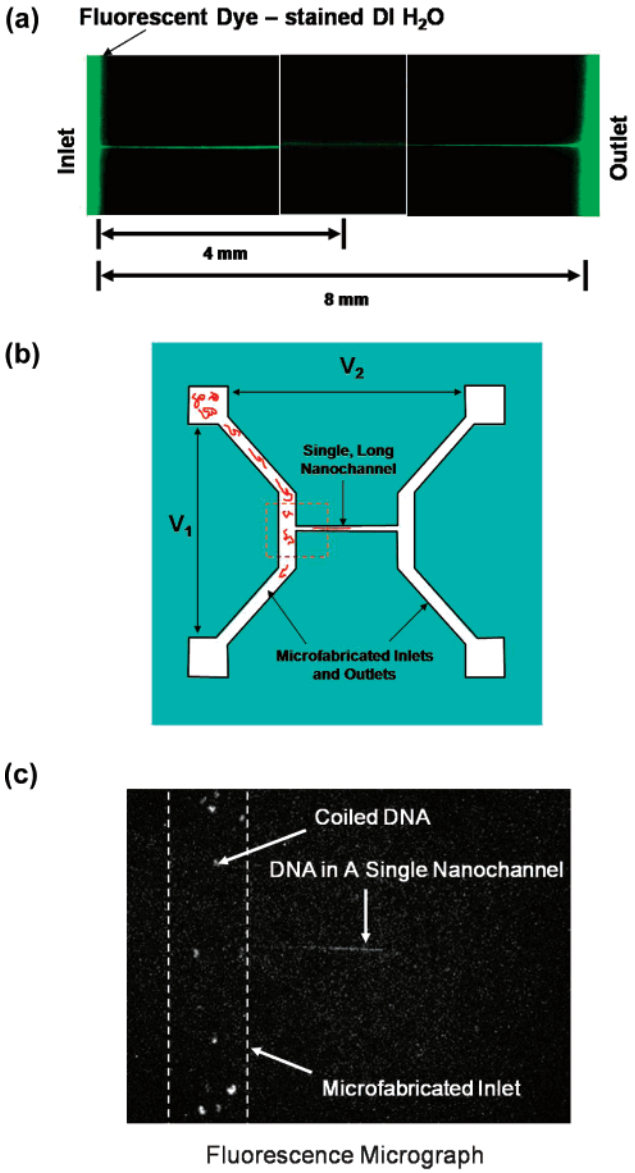

Figure 5. (a) Continuous water flow with fluorescent dye through a 30 nm wide, 8 mm long single nanochannel. (b) Schematic of a single narrow long nanochannel and its inlets and outlets. (c) A video frame capture of a stretched T2 DNA moving through a 3 mm long, 50 nm square nanochannel driven by electrophoretic force.

middle point (x = 4 mm), and the outlet (x = 8 mm), respectively, using an inverted microscope (Nikon TE-300 equipped with Nikon Plan Apo 60×/1.40 oil lens). We carefully scanned the whole nanochannel and ensured that the fluorescent signal is detectable and continuous everywhere along the entire nanochannel, which indicates a channel continuity over the entire channel length.

In testing the narrow long channel using DNAs in a solution, we used a 50 nm wide, 3 mm long nanochannel. The sealed channel was wet with a loading buffer (0.045 M tris-base, 1 mM EDTA with 0.045 M boric acid (0.5 × TBE)). An oxygen scavenging system (4 mg/mL β−D glucose, 0.2 mg/mL glucose oxidase, 0.04 mg/mL catalase and 0.07 M β-mercaptoethanol) was also added to suppress the bleaching of DNAs. The DNA was labeled with TOTO-1

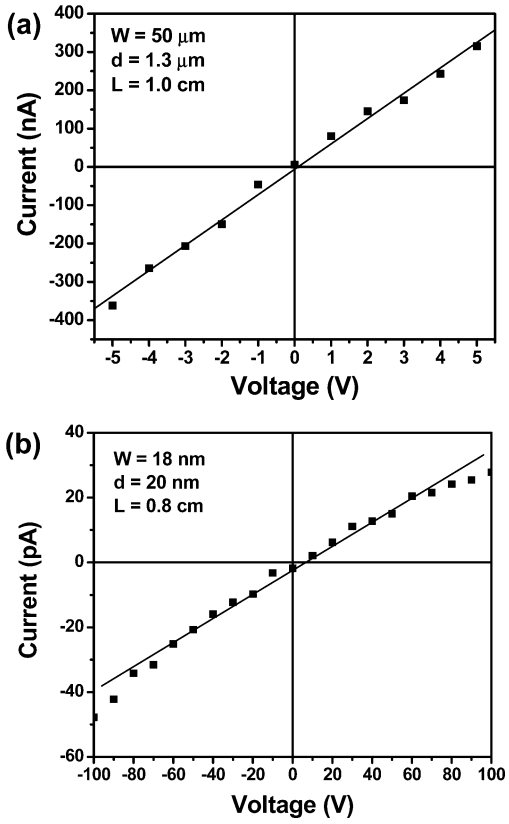

Figure 6. The I−V characteristic of a salt solution (1 M KCl, 10 mM Tris-base, pH = 8.0) along (a) a 50 μm wide, 1.3 μm deep, 1.0 cm long microfluidic channel, and (b) an 18 nm wide, 20 nm deep, 0.8 cm long nanofluidic channel in SiO_2.

fluorescent dye (Molecular Probes) at a concentration of 1 dye molecule per every 10 base pairs. Electrophoresis was used to move genomic length T2 DNA (164 kbp) in the device. As schematically shown in Figure 5b, the DNAs were first guided in a microchannel inlet by a mild voltage ($V_1 \sim$ 10 V). Once the DNA approached to the interface between the microchannel and the nanochannel, a higher voltage ($V_2 \sim$ 50 V) was applied across the whole nanochannel to stretch the DNA into the nanochannel. A video frame capture of DNA (Figure 5c) shows that a DNA was stretched as it moves into and through the nanochannel. The captured video shows a continuous motion of this stretched DNA in the nanochannel, indicating the channel continuity over the entire channel length. The fluorescent DNA image in the video frame is rather faint compared with a static image observed in a short and multiple channels system,[32] because the electropheretic force drives the DNA swiftly moves across the whole imaging range. Presently, we are unable to flow T2 DNAs into the sub-20 nm channels by electrophoresis, but we believe that that is caused by a large entropic barrier (due to an abrupt change of channel width at the narrow channel inlet) and the effect of the surface charge.[33]

To confirm the sub-20 nm channel cross-section, we measured the electrical conductance of a salt solution (1 M KCl, 10 mM tris, pH = 8.0) along an 18 nm wide, 20 nm deep, 0.8 cm long nanofluidic channel as well as a 50 μm wide, 1.3 μm deep, 1 cm long microfluidic channel. The microchannel of its well-calibrated channel cross-section

served as a control to give the salt solution conductivity, which was then used to calculate the cross-section of the nanochannel with the known channel length. All electrical measurements were at room temperature using a pA meter/DC source (HP 4140B). Figure 6a shows the I−V characteristic in the microchannel, and electrical conductance was extracted to be $G_m = 66.1$ nS by fitting experimental data (solid squares). On the basis of the microchannel dimensions ($w = 50$ μm, $d = 1.3$ μm, $L = 1$ cm), the electrical conductivity of the salt solution was found to be $\sigma = G_m L/wd = 10.2$ S/m, which is consistent with those reported elsewhere.[34] Using this conductivity together with the electrical conductance of 0.40 pS of the same salt solution in the nanochannel measured from its I−V characteristic (Figure 6b), the channel cross-section is 314 nm^2 (namely, 17.7 nm × 17.7 nm), offering another independent experimental validation of both the nanometer channel cross-section and the fluidic continuity of the centimeter-long sub-20 nm nanochannel. The calculation used the channel length of $L = 0.8$ cm, which was measured by optical microscopy, and does not consider the Debye screening effect (for 1 M KCl solution, the Debye screening length $\lambda_D \sim 0.3$ nm).[35]

In summary, the new approach we proposed has clearly demonstrated the fabrication of a single, narrow (as small as 11 nm), long (over 1.5 cm) and continuous fluidic channel and the transporting and stretching of DNAs in these channels. The new approach has removed a key obstacle and hence has opened the door for developing a variety of innovative bio/chemical sensors, particularly single-stranded DNA sequencing devices.

Acknowledgment. The work was supported in part by DARPA.

References

(1) Stern, M. B.; Geis, M. W.; Curtin, J. E. *J. Vac. Sci. Technol., B* **1997**, *15* (6), 2887−2891.
(2) Austin, R. H.; Tegenfeldt, J. O.; Cao, H.; Chou, S. Y.; Cox, E. C. *IEEE Trans. Nanotechnol.* **2002**, *1* (1), 12−18.
(3) Ilic, B.; Czaplewski, D.; Zalalutdinov, M.; Schmidt, B.; Craighead, H. G. *J. Vac. Sci. Technol., B* **2002**, *20* (6), 2459−2465.
(4) Cannon, D. M.; Flachsbart, B. R.; Shannon, M. A.; Sweedler, J. V.; Bohn, P. W. *Appl. Phys. Lett.* **2004**, *85* (7), 1241−1243.
(5) Fan, R.; Karnik, R.; Yue, M.; Li, D. Y.; Majumdar, A.; Yang, P. D. *Nano Lett.* **2005**, *5* (9), 1633−1637.
(6) Mijatovic, D.; Eijkel, J. C. T.; van den Berg, A. *Lab Chip* **2005**, *5* (5), 492−500.
(7) Lagerqvist, J.; Zwolak, M.; Di Ventra, M. *Nano Lett.* **2006**, *6* (4), 779−782.
(8) Groves, T. R.; Pickard, D.; Rafferty, B.; Crosland, N.; Adam, D.; Schubert, G. *Microelectron. Eng.* **2002**, *61−2*, 285−293.
(9) Melngailis, J.; Mondelli, A. A.; Berry, I. L.; Mohondro, R. *J. Vac. Sci. Technol., B* **1998**, *16* (3), 927−957.
(10) McCord, M. A.; Pease, R. F. W. *Appl. Phys. Lett.* **1987**, *50* (10), 569−570.
(11) Mannion, J. T.; Reccius, C. H.; Cross, J. D.; Craighead, H. G. *Biophys. J.* **2006**, *90* (12), 4538−4545.
(12) Fan, R.; Yue, M.; Karnik, R.; Majumdar, A.; Yang, P. D. *Phys. Rev. Lett.* **2005**, *95* (8).
(13) Zwolak, M.; Di Ventra, M. *Nano Lett.* **2005**, *5* (3), 421−424.
(14) Chou, S. Y. Princeton University, Princeton, NJ, Unpublished work, 2004.
(15) O'Brien, M. J.; Bisong, P.; Ista, L. K.; Rabinovich, E. M.; Garcia, A. L.; Sibbett, S. S.; Lopez, G. P.; Brueck, S. R. J. *J. Vac. Sci. Technol., B* **2003**, *21* (6), 2941−2945.
(16) Dumond, J. J.; Low, H. Y.; Rodriguez, I. *Nanotechnology* **2006**, *17* (8), 1975−1980.
(17) Tegenfeldt, J. O.; Cao, H.; Reisner, W. W.; Prinz, C.; Austin, R. H.; Chou, S. Y.; Cox, E. C.; Sturm, J. C. *Biophys. J.* **2004**, *86* (1), 596A−596A.
(18) Lee, C.; Yang, E. H.; Myung, N. V.; George, T. *Nano Lett.* **2003**, *3* (10), 1339−1340.
(19) Choi, Y. K.; Lee, J. S.; Zhu, J.; Somorjai, G. A.; Lee, L. P.; Bokor, J. *J. Vac. Sci. .Technol., B* **2003**, *21* (6), 2951−2955.
(20) Czaplewski, D. A.; Kameoka, J.; Mathers, R.; Coates, G. W.; Craighead, H. G. *Appl. Phys. Lett.* **2003**, *83* (23), 4836−4838.
(21) Verbridge, S. S.; Edel, J. B.; Stavis, S. M.; Moran-Mirabal, J. M.; Allen, S. D.; Coates, G.; Craighead, H. G. *J. Appl. Phys.* **2005**, *97* (12).
(22) Wang, M.; Jing, N.; Su, C. B.; Kameoka, J.; Chou, C. K.; Hung, M. C.; Chang, K. A. *Appl. Phys. Lett.* **2006**, *88* (3).
(23) Wong, C. C.; Agarwal, A.; Balasubramanian, N.; Kwong, D. L. *Nanotechnology* **2007**, *18* (13).
(24) Cao, H.; Yu, Z. N.; Wang, J.; Tegenfeldt, J. O.; Austin, R. H.; Chen, E.; Wu, W.; Chou, S. Y. *Appl. Phys. Lett.* **2002**, *81* (1), 174−176.
(25) Wang, Y. M.; Tegenfeldt, J. O.; Reisner, W.; Riehn, R.; Guan, X. J.; Guo, L.; Golding, I.; Cox, E. C.; Sturm, J.; Austin, R. H. *Proc. Natl. Acad. Sci. U.S.A.* **2005**, *102* (28), 9796−9801.
(26) Hug, T. S.; de Rooij, N. F.; Staufer, U. *Microfluid. Nanofluid.* **2006**, *2* (2), 117−124.
(27) Chou, S. Y. Princeton University, Princeton, NJ, Unpublished work, 2005.
(28) Chou, S. Y.; Smith, H. I.; Antoniadis, D. A. *J. Vac. Sci. Technol., B* **1985**, *3* (6), 1587−1589.
(29) Chou, S. Y.; Krauss, P. R.; Renstrom, P. J. *Appl. Phys. Lett.* **1995**, *67* (21), 3114−3116.
(30) Chou, S. Y.; Krauss, P. R.; Renstrom, P. J. *Science* **1996**, *272* (5258), 85−87.
(31) Constantoudis, V.; Patsis, G. P.; Tserepi, A.; Gogolides, E. *J. Vac. Sci. Technol., B* **2003**, *21* (3), 1019−1026.
(32) Reisner, W.; Morton, K. J.; Riehn, R.; Wang, Y. M.; Yu, Z. N.; Rosen, M.; Sturm, J. C.; Chou, S. Y.; Frey, E.; Austin, R. H. *Phys. Rev. Lett.* **2005**, *94* (19).
(33) Cao, H.; Tegenfeldt, J. O.; Austin, R. H.; Chou, S. Y. *Appl. Phys. Lett.* **2002**, *81* (16), 3058−3060.
(34) Stein, D.; Kruithof, M.; Dekker, C. *Phys. Rev. Lett.* **2004**, *93* (3).
(35) Israelachvili, J. *Intermolecular and Surface Forces*, 2nd ed.; Academic Press: London, 2003. For 1:1 electrolyte solution, the Debye screening length $\lambda_D \sim 0.307/\sqrt{C_b}$ [unit: nm] at room temperature, where C_b is bath concentration [unit: M].

NL072253X